ACS EARTH AND SPACE CHEMISTRY

http://pubs.acs.org/journal/aesccq

Article

Thermochemistry and Kinetics of the OH- and Cl-Initiated Degradation Pathways of the HCFC-132b Atmospheric Pollutant

Nadjib Rais, Zoi Salta, and Nicola Tasinato*

Cite This: *ACS Earth Space Chem.* 2023, 7, 892−900

Read Online

ACCESS | Metrics & More | Article Recommendations | Supporting Information

ABSTRACT: The gas-phase hydrogen abstraction reaction of 1,2-dichloro-1,1-difluoroethane ($CH_2ClCClF_2$) with OH and Cl radicals is theoretically investigated by employing density functional theory methods combined with coupled-cluster-based composite schemes. The mechanism and kinetics of the degradation entrance channels of $CH_2ClCClF_2$, recently detected with increasing concentration in the atmosphere, is elucidated by using cost-effective ab initio triple-slash dual-level direct dynamics, jChS//B2PLYP-D3(BJ)/jun-cc-pV(T+d)Z///M06-2X-D3/jun-cc-pV(T+d)Z. Thermal rate constants are calculated over the temperature range of 200−1000 K by adopting both canonical- (CVT) and microcanonical (μVT)-variational transition state theory also including the microcanonically optimized multidimensional tunneling transmission coefficient (μOMT). The theoretical rate coefficient for the H-abstraction reaction initiated by the OH radical is computed to be $k_{OH}^{CVT/\mu OMT} = 1.72 \times 10^{-14}$ cm^3 molecule^{-1} s^{-1} and $k_{OH}^{\mu VT/\mu OMT} = 1.57 \times 10^{-14}$ cm^3 molecule^{-1} s^{-1} at 298 K, in excellent agreement with the available experimental data. The rate constant for the H-abstraction reaction by the Cl atom, here obtained for the first time, is predicted to be $k_{Cl}^{CVT/\mu OMT} = 5.96 \times 10^{-14}$ cm^3 molecule^{-1} s^{-1} and $k_{Cl}^{\mu VT/\mu OMT} = 5.65 \times 10^{-14}$ cm^3 molecule^{-1} s^{-1} at 298.15 K, thus showing increased efficiency with respect to the OH-prompted reaction.

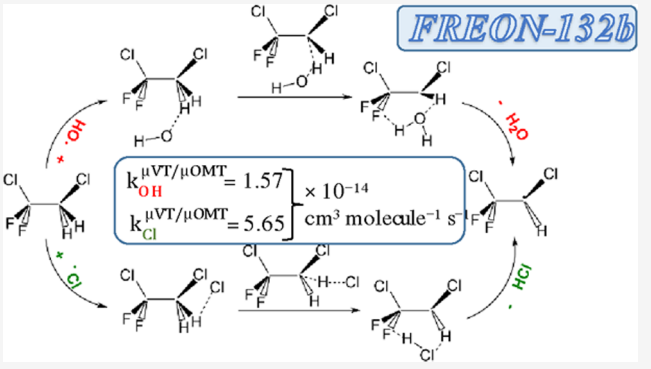

KEYWORDS: *atmospheric chemistry, halogenated organics, environmental pollutants, computational chemistry, intermolecular hydrogen transfer*

Downloaded via SCUOLA NORMALE SUPERIORE DI PISA on April 28, 2023 at 12:16:44 (UTC).
See https://pubs.acs.org/sharingguidelines for options on how to legitimately share published articles.

1. INTRODUCTION

Hydrochlorofluorocarbons (HCFCs) were adopted in the late 1980s as direct substitutes of chlorofluorocarbons (CFCs) since the use of latter compounds was prohibited by the Montreal Protocol.[1] CFCs were widely used as refrigerants, blowing agents, solvent, and insulators; however, because of their high chemical and thermal stability, they diffuse to the stratosphere where UV irradiation causes the homolytic dissociation of the C−Cl bond. The ensuing Cl atom then destroys stratospheric ozone in a catalytic process of chain reactions.[2] The introduction of HCFCs as alternatives to CFCs aimed at exploiting their shorter atmospheric lifetimes, thus ensuring that a smaller fraction of the emitted amount is transported to the stratosphere. This feature comes from the presence of C−H bonds in the molecule that makes them reactive toward the oxidant species present in the troposphere (mostly hydroxyl and chlorine radicals). Therefore, the ozone depletion potential (ODP) of HCFCs is much smaller than that of CFCs. HCFCs, however, present strong absorptions in the infrared spectral region (very notably within the 8−12 μm atmospheric window), and hence they can contribute to global warming.[3] Consequently, the Montreal protocol amendment in 2007 was designed to gradually reduce their use and completely phase them out (by 2020 for developed countries and 2030 for developing countries).

Irrespective of the mentioned regulations, very recently, an international network of climate scientists detected an increasing atmospheric concentration of 1,2-dichloro-1,1-difluoroethane ($CH_2ClCClF_2$),[4] also known as HCFC-132b or Freon-132b, which was initially intended as a replacement for CFC-113 ($CF_2ClCFCl_2$) in different industrial applications.[5−7] While some investigations on its properties and photochemical processes have been performed over the years,[8−12] to the best of our knowledge, those involving the mechanisms and kinetics of reactions relevant to atmospheric chemistry are very limited.

Initially, Watson et al.[13] studied the kinetics of the reaction between HCFC-132b and OH radicals (reaction R1) in the temperature range of 250−350 K, by flash-photolysis resonance fluorescence obtaining an effective Arrhenius equation for the

Received: January 23, 2023
Revised: March 2, 2023
Accepted: March 13, 2023
Published: March 27, 2023

ACS Publications

© 2023 The Authors. Published by American Chemical Society

rate constant characterized, however, by a quite large uncertainty interval in the derived exponential and preexponential factors. Subsequently, the same reaction was reinvestigated in the temperature range of 249−473 K using the discharge-flow technique,[14] resulting in the following Arrhenius equation (in cm^3 $molecule^{-1}$ s^{-1}): $k_{OH} = 5.54 \times 10^{-26} T^{4.58} \exp\{-(252 \pm 377)/T\}$. With the aim of extending the temperature range of the rate equation, Fang et al.[15] performed an additional study over the temperature interval of 295−788 K by means of laser photolysis/laser-induced fluorescence (PLP/LIF), deriving the following Arrhenius equation: $k_{OH} = (8.53 \pm 4.06) \times 10^{-19} T^{2.28} \exp\{-(937 \pm 296)/T\}$ in cm^3 $molecule^{-1}$ s^{-1}.

$$CH_2ClCClF_2 + OH \rightarrow CHClCClF_2 + H_2O \quad (R1)$$

While the OH-initiated oxidation has been widely experimentally investigated by different research groups, the kinetic details of the reaction between HCFC-132b and the Cl atom (reaction R2) have never been determined either experimentally or theoretically. In this respect, it is worth mentioning that the Cl-atom-initiated degradation of some HCFCs and HFCs has been studied with regard to both reaction rate coefficient measurements and the identification of stable end-products,[16−18] leading to the conclusion that Cl-atom reaction rate coefficients are greater than those of the analogous OH reactions for both abstraction and addition processes. Thus, the increased Cl atom reactivity may compensate to some extent for its atmospheric abundance being lower than the OH radical, and it can impact the overall degradation rates of HCFCs and HFCs in the troposphere, especially in the coastal regions where the abundance of Cl atoms is higher.

$$CH_2ClCClF_2 + Cl \rightarrow CHClCClF_2 + HCl \quad (R2)$$

Due to the unexpected increase in the atmospheric concentration of HCFC-132b, each reaction relevant to its atmospheric chemistry and each process that contribute to determining the overall atmospheric lifetime need to be carefully characterized and understood. This implies investigating the reaction pathways leading to atmospheric degradation, with careful examination of the possible intermediates and products, starting from the reactions involving the most important OH and Cl atmospheric scavengers, also with the aim of understanding the environmental impact of this compound. With these premises, in this work, we undertake the theoretical investigation of the entrance channel for the degradation of HCFC-132b initiated by the OH and Cl radicals, in order to shed light on the corresponding reaction mechanisms and fill the actual gaps in the available thermochemical and kinetic data.

2. COMPUTATIONAL METHODS

The $CH_2ClCClF_2$ + OH (reaction R1), and $CH_2ClCClF_2$ + Cl (reaction R2) reactions were investigated by employing triple-slash dual-level (X//Y///Z) direct dynamics calculations[19−21] over a temperature range of 200−1000 K. In this methodology, the path-reaction swath data for calculating the optimized multidimensional tunneling were computed at a lower-level Z, rotational constants and Hessians were evaluated at an intermediate level Y, and single-point electronic energies were refined at a high level of theory X. Theoretical rate constants were calculated using variational transition state theory (VTST)[22] in both canonical and microcanonical frameworks including semiclassical multidimensional tunneling.[23] More in detail, the mapping of the potential energy surface (PES) was performed first using the hybrid meta-GGA M06-2X functional[24] augmented by DFT-D3 Grimme's dispersion corrections with zero damping,[25] in conjunction with the jun-cc-pV(T+d)Z basis set,[26] which includes an additional set of polarization *d* functions, required to achieve a consistent description of second-row elements.[27,28] The stationary points on the M06-2X-D3 PES were characterized through the computation of analytical second-order derivatives. The M06-2X-D3 minimum energy path (MEP) was followed in mass-scaled Cartesian coordinates by the Page−McIver method[29] using a step size of 0.003 au and a scaling mass of 1 amu, with molecular Hessians calculated at each step. The normal-mode analysis was performed in redundant curvilinear coordinates,[30] to avoid spurious small imaginary frequencies that appear when working in cartesian coordinates.

Following a well-consolidated procedure,[31−33] equilibrium geometries (and hence moments of inertia) and harmonic vibrational frequencies of the stationary points on the reactive PES were refined by using the B2PLYP double hybrid functional,[34] augmented by DFT-D3 dispersion with Becke−Johnson damping,[35,36] in conjunction with jun-cc-pV(T+d)Z basis set. This level of theory has been demonstrated to provide a very good trade-off between accuracy and computational cost, providing equilibrium geometries and vibrational frequencies of about the same quality as coupled cluster with singles, doubles, and perturbative triples, CCSD(T), coupled to a triple-ζ basis set.[37−40] Finally, electronic energies of the stationary points on the PES were further improved by applying the recently developed composite scheme "jun-cheap" (jChS)[41,42] on top of B2PLYP-D3/jun-cc-pV(T+d)Z geometries. While interested readers are referred to the specific literature for a complete account, here we only mention that the jChS starts from the CCSD(T)/jun-cc-pV(T+d)Z energy within the frozen-core approximation that is improved by the extrapolation to the complete basis set (CBS limit)[43] and the inclusion of core-valence (CV) correlation performed using the Møller−Plesset second-order perturbation theory.[44]

Thermal rate constants of the reactions investigated were computed by means of variational transition state theory with interpolated optimized corrections (VTST-IOC)[45] over the 200−1000 K temperature range using both the canonical (CVT) and microcanonical (μVT) formulations.[46,47] CVT rate constants are given by

$$k^{CVT}(T) = \min_s k^{GT}(T, s) \quad (1)$$

$$k^{GT}(T, s) = \sigma \frac{Q(T, s)}{\beta h \Phi^R(T)} \exp(-\beta V_{MEP}(s)) \quad (2)$$

where σ is the reaction path degeneracy; β stands for $(K_B T)^{-1}$, with K_B and T being, respectively, the Boltzmann constant and the temperature; h is Planck's constant; $\Phi^R(T)$ is the reactants' partition function product per unit volume; $V_{MEP}(s)$ is the classical energy along the minimum energy path (MEP) s; and $Q(T, s)$ is the product of the rotational, vibrational, and electronic partition functions of the generalized transition state. According to μVT, which improves CVT by considering that the reactants are equilibrated microcanonically (in a fixed-energy ensemble) rather than canonically, the rate constant expression is defined as

$$N^{\mu VT}(E) = \min_s \{N^{GT}(E, s)\} \quad (3)$$

https://doi.org/10.1021/acsearthspacechem.3c00025
ACS Earth Space Chem. 2023, 7, 892−900

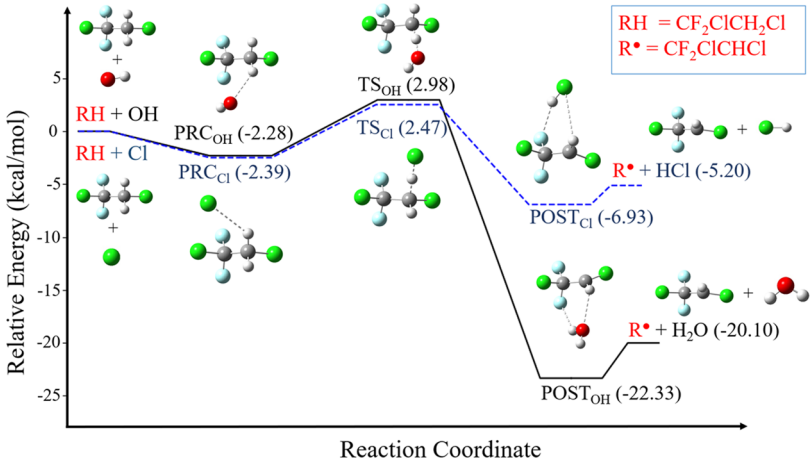

Figure 1. Reactive PES of the H-abstraction reactions from $CH_2ClCClF_2$ by the OH (black, solid) and Cl (blue, dashed) radicals, using the B2PLYP-D3(BJ) ZPE-corrected jChS relative energies (kcal mol^{-1}).

$$k^{\mu VT}(T) = \sigma \frac{N^{\mu VT}(E)}{h\rho(E)} \quad (4)$$

where $N^{\mu VT}(E)$ is the sum over states of the transition state obtained by variationally minimizing N^{GT} (i.e., the number of states at a given generalized transition state) with respect to the reaction coordinate s and $\rho(E)$ is the density of states (DOS) of the reactants.

Quantum tunneling was also included by multiplying CVT and μVT rate constants by a transmission coefficient k_T calculated by the microcanonically optimized multidimensional tunneling (μOMT),[48] which chooses the largest value between the small-curvature tunneling (SCT),[49−52] and the large-curvature tunneling (LCT).[48,51,53−58] The LCT was evaluated with the LCT method (version 4),[58] using the interpolated large-curvature tunneling in two dimensions (ILCT2D) algorithm.[59] The reason for including the μOMT tunneling is that the skew angles β (defined, for a typical reaction A + BC → AB + C, as $\varphi = \cos^{-1}\sqrt{m_A m_C/(m_A + m_B)(m_C + m_B)}$, with m_i mass of the species i of the reactions under study) were found around 15° for (reaction R1) and 11° for (reaction R2), which indicate that the reaction path curvature is large.[60] In the following, acronyms TST, CVT, and μVT are used to, respectively, denote conventional transition state theory, canonical variational transition state theory, and microcanonical variational transition state theory results without tunneling. The calculated rate coefficients in the 200−1000 K temperature range were then fitted to a modified Arrhenius equation of the type

$$k = AT^n \exp\left(\frac{-E_a}{RT}\right) \quad (5)$$

All quantum chemical calculations were performed using the Gaussian16 suite of programs,[61] while direct dynamics computations were carried out using Polyrate 2017-C[62] and Gaussrate 17-B[63] codes.

3. RESULTS AND DISCUSSION

3.1. Thermodynamic Evaluation. The mechanism of the OH- and Cl-initiated H-abstraction reactions of HCFC-132b is depicted in Figure 1, and the geometries of the stationary points are collected in Figure 2, where some representative structural parameters are also reported. Relative electronic and ZPVE-corrected energies with respect to the separated reactants obtained at the levels of theory used in this study are listed in Table 1.

3.1.1. H-Abstraction by the OH Radical. The OH + $CH_2ClCClF_2$ reaction (reaction R1) is expected to occur through direct H-abstraction from the $-CH_2Cl$ group. The reaction proceeds via an S_H2-type pre-reactive complex PRC_{OH} (Figure 2), which features an intermolecular H-bond between the oxygen lone pair of the radical and one of the two equivalent hydrogen atoms of the CH_2Cl group. Then, by overcoming a barrier of about 3 kcal mol^{-1} passing through TS_{OH}, the "three-centers/four-electrons" post-reactive complex $POST_{OH}$ is reached, which subsequently releases the $CHClCClF_2$ radical and H_2O as products. As seen in Table 1, at the jChS//B2PLYP/jun-cc-pV(T+d)Z level of theory, the pre-reactive complex PRC_{OH} is at a ZPVE-corrected energy of about 2.3 kcal mol^{-1} below the reactants, whereas the post-reactive complex $POST_{OH}$ is about 22.3 kcal mol^{-1} more stable than the reactants and about 2.2 kcal mol^{-1} more stable than the separated products. These complexes are stabilized by the hydrogen bond attractive interaction, as evidenced by the fact that they are lower in energy than reactants and products, respectively. It has to be noted that both pre- and post-reactive complexes need to be considered in gas-phase kinetics simulations since their presence narrows the width of the reaction barrier, significantly affecting the tunneling contribution to the rate coefficients. Overall, the reaction R1 is predicted to be exothermic by −20.1 kcal mol^{-1} according to the jChS corrected for ZPVE contributions evaluated at the B2PLYP level of theory.

3.1.2. H-Abstraction by the Cl Atom. The reaction between $CH_2ClCClF_2$ and Cl (reaction R2) proceeds, analogously to (reaction R1), via the direct H-abstraction from the CH_2Cl group. As reported in Figure 1, it involves pre- (PRC_{Cl}) and post-reactive ($POST_{Cl}$) complexes, which have a relative energy with respect to reactants of −2.4 and −6.9 kcal mol^{-1} at the jChS//B2PLYP/jun-cc-pV(T+d)Z level of theory, respectively. In these complexes, the Cl atom weakly interacts with the hydrogen atoms of the $-CH_2Cl$ group. The optimized structures of these complexes as well as of products and the connecting transition state are given in Figure 2 together with selected bond distances. As can be seen in Table 1, the reaction is exothermic by −5.2 kcal mol^{-1}, presenting a forward barrier height of 2.5 kcal mol^{-1}.

https://doi.org/10.1021/acsearthspacechem.3c00025
ACS Earth Space Chem. 2023, 7, 892−900

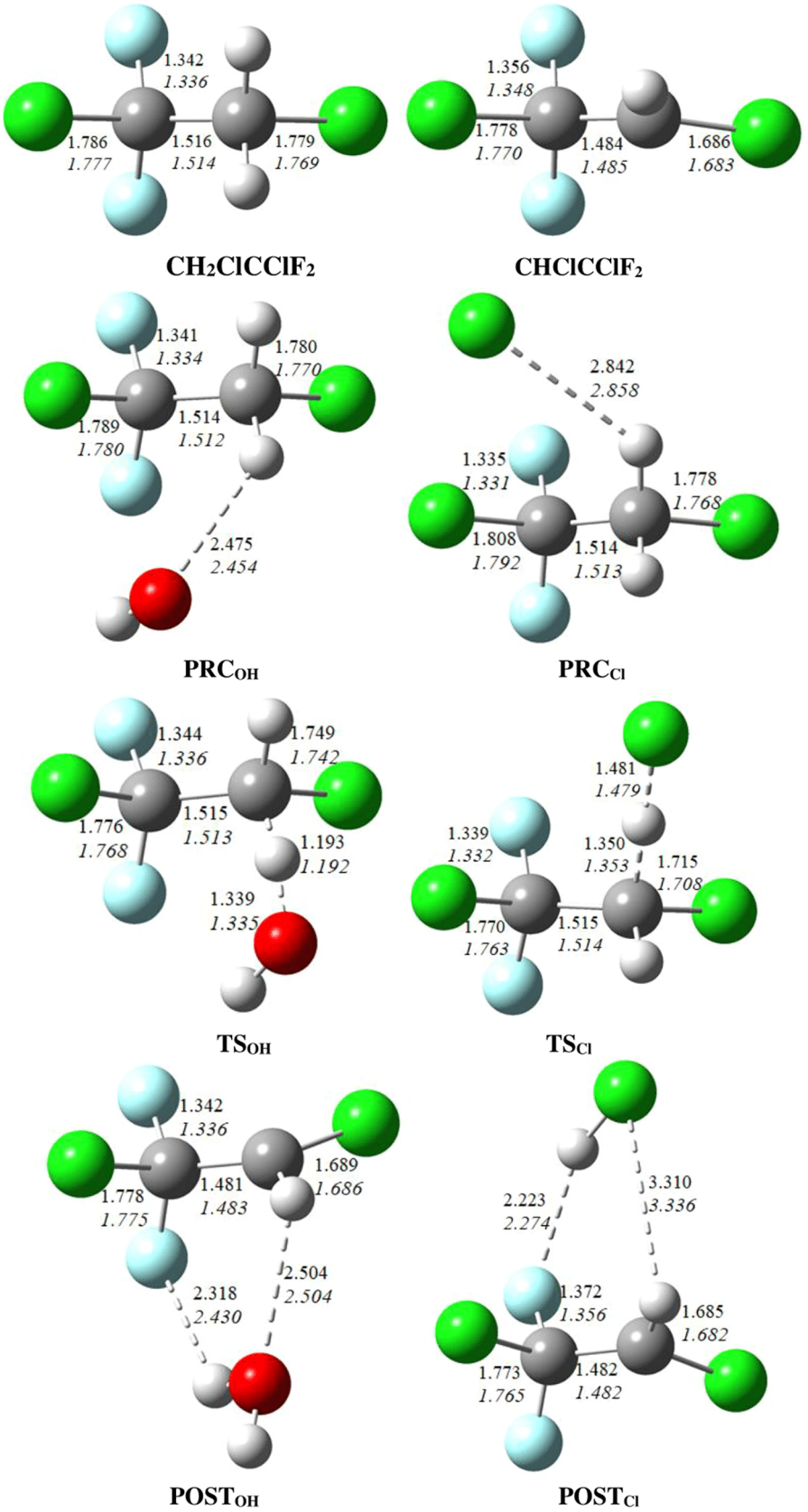

Figure 2. Optimized geometries of the species in the reactive PES for the OH- and Cl-initiated H-abstraction from $CH_2ClCClF_2$ at B2PLYP-D3(BJ)/jun-cc-pV(T+d)Z and M06-2X-D3/jun-cc-pV(T+d)Z (in italics) levels of theory. Representative bond distances (Å) are also reported.

Before moving to the assessment of the chemical kinetics, it is interesting to note that the difference of the enthalpies of reactions R1 and R2 is the enthalpy of the reaction OH + HCl → H_2O + Cl. According to the present calculations, the latter has

https://doi.org/10.1021/acsearthspacechem.3c00025
ACS Earth Space Chem. 2023, 7, 892−900

Table 1. Relative Electronic (ΔE) and Ground-State $\Delta(E + ZPVE)$ Energies (kcal mol^{-1}) of the Stationary Points on the Reactive PES for the OH- and Cl-Initiated H-Abstraction from $CH_2ClCClF_2$

	ΔE			$\Delta(E + ZPVE)$		
	M06-2X[a]	B2PLYP[a]	jChS	M06-2X[b]	B2PLYP[c]	jChS[d]
R1: $CH_2ClCClF_2$ + OH	0.00	0.00	0.00	0.00	0.00	0.00
PRC_{OH}	−4.50	−3.12	−3.14	−3.41	−2.26	−2.28
TS_{OH}	4.19	3.18	4.96	2.33	1.20	2.98
$POST_{OH}$	−22.46	−22.33	−22.65	−22.06	−22.05	−22.37
$CHClCClF_2$ + H_2O	−18.18	−18.84	−19.13	−19.08	−19.81	−20.10
R2: $CH_2ClCClF_2$ + Cl	0.00	0.00	0.00	0.00	0.00	0.00
PRC_{Cl}	−3.83	−3.38	−2.67	−3.51	−3.10	−2.39
TS_{Cl}	6.13	5.14	7.04	1.45	0.57	2.47
$POST_{Cl}$	−2.91	−3.29	−3.04	−6.72	−7.18	−6.93
$CHClCClF_2$ + HCl	0.11	−0.63	−0.43	−4.64	−5.40	−5.20

[a]In conjunction with the jun-cc-pV(T+d)Z basis set. [b]Electronic and ZPVE at the M06-2X-D3/jun-cc-pV(T+d)Z level. [c]Electronic and ZPVE at the B2PLYP-D3(BJ)/jun-cc-pV(T+d)Z level. [d]jChS electronic energy corrected for ZPVE at the B2PLYP-D3(BJ)/jun-cc-pV(T+d)Z level.

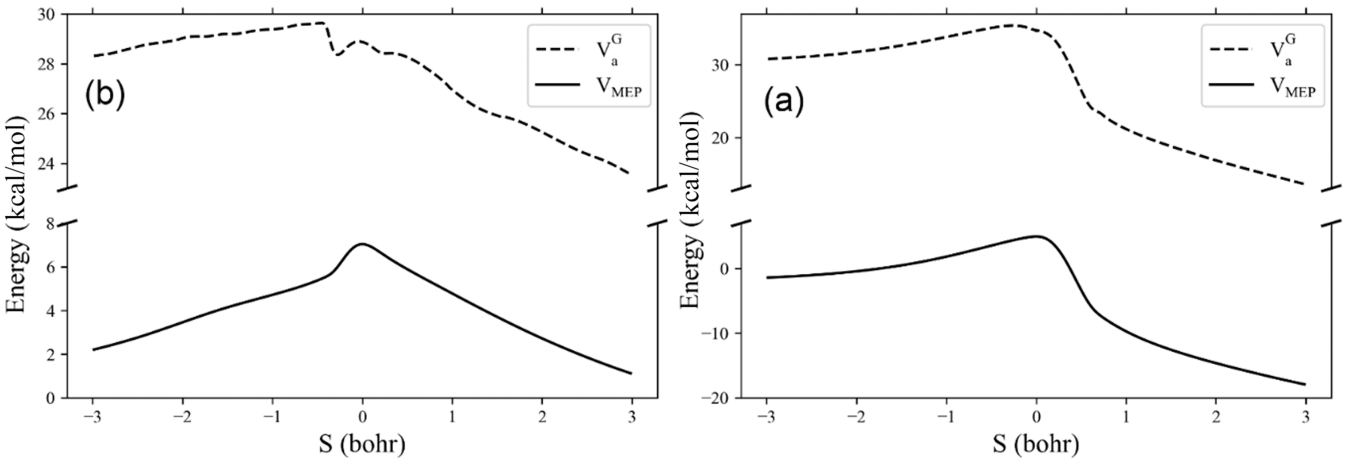

Figure 3. Classical potential energy curve (V_{MEP}, solid) and ground-state vibrationally adiabatic energy curve (V_a^G, dotted line) as a function of s at the jChS//B2PLYP-D3(BJ)/jun-cc-pV(T+d)Z///M06-2X-D3/jun-cc-pV(T+d)Z level of theory, for the HCFC-132b H-abstraction reaction initiated by OH (a) and Cl (b).

resulted to be −14.9 kcal mol^{-1} in good agreement with the value listed in the Active Thermochemical Tables (ATcT),[64] thus providing further support to the reliability and accuracy of the adopted approach.

3.2. Kinetic Results. *3.2.1. Reaction Path Degeneracy.* On the basis of the mechanisms described above, the reaction path symmetry factor, σ, for reactions R1 and R2, which accounts for the number of equivalent reaction paths, was taken into account according to the general expression[54,65]

$$\sigma = \frac{n_{TS}\sigma_R}{n_R\sigma_{TS}} \quad (6)$$

where n_{TS} and n_R are the number of enantiomers and σ_{TS} and σ_R are the symmetry numbers of the transition state and the reactants, respectively. The symmetry point groups for the reactants are C_S for $CH_2ClCClF_2$ and $C_{\infty v}$ for OH, yielding σ_R = 1, and the Cl symmetry number is also 1, being an isolated atom. The symmetry point group for both transition states is C_1, leading to σ_{TS} = 1. The number of enantiomers for the reactants is 1, whereas the transition state has two enantiomers, hence the symmetry number for reactions R1 and R2 is 2. Hereafter, all of the theoretical rate constants are multiplied by a factor of 2 to consider the reaction path degeneracy.

3.2.2. Reaction Path Properties. The MEP calculations for each reaction were performed based on triple-slash dual-level direct dynamics using the jChS//B2PLYP-D3(BJ)/jun-cc-pV(T+d)Z///M06-2X-D3/jun-cc-pV(T+d)Z level of theory within the VTST-IOC approach. The overall flux for the reactions R1 and R2 is solely determined by the H-abstraction step, meaning that, the dynamical association process that leads to the pre-reactive complex is not considered kinetically relevant. However, as mentioned before, pre- and post-reactive complexes do influence the tunneling transmission coefficient and the variational characteristics of the transition state. The importance of these complexes has already been pointed out,[66−68] and therefore they are explicitly taken into account in the kinetics calculations performed by the Polyrate program. The classical potential energy curve, V_{MEP}, and the ground-state vibrationally adiabatic potential energy curve, V_a^G, as a function of the distance along the MEP for reactions R1 and R2 are shown in Figure 3. The location of the maximum on the $V_a^G(s)$ curve for reaction R1 is comparable with the V_{MEP} curve, so the variational effect for this reaction is unlikely to be important. On the contrary, for reaction R2, the maximum of $V_a^G(s)$ is shifted in the s direction toward the reactants, thus suggesting that variational effects can be significant.

3.2.3. Thermal Rate Constants. The thermal rate constants obtained by CVT/μOMT and μVT/μOMT methods for the H-abstraction reactions over the temperature range 200−1000 K are shown in Figure 4, whereas Table S2 in the Supporting

https://doi.org/10.1021/acsearthspacechem.3c00025
ACS Earth Space Chem. 2023, 7, 892−900

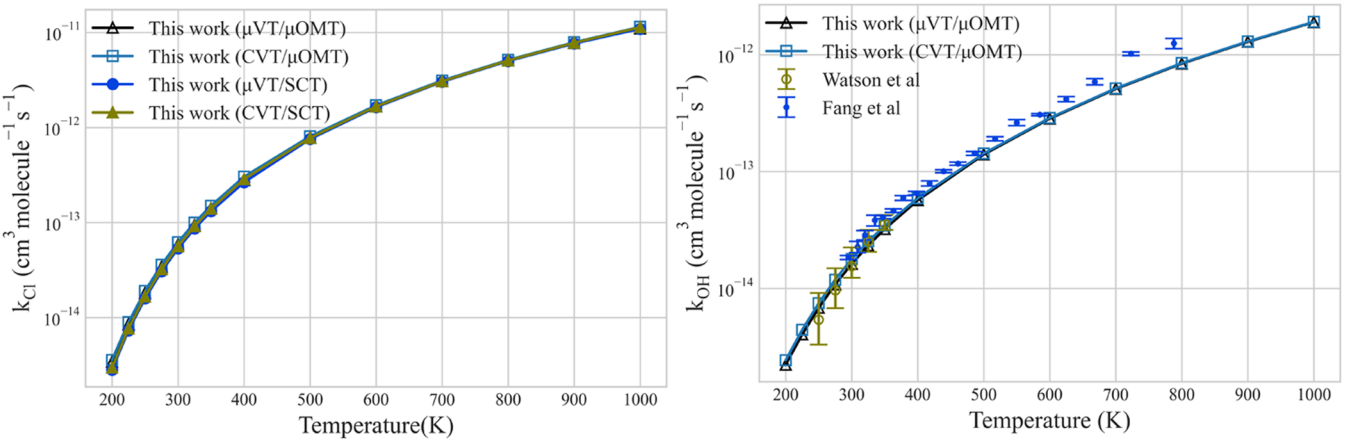

Figure 4. Calculated rate coefficients at the jChS//B2PLYP-D3(BJ)/jun-cc-pV(T+d)Z///M06-2X-D3/jun-cc-pV(T+d)Z level of theory between 200 and 1000 K for the $CH_2ClCClF_2$ + OH reaction (right) and the $CH_2ClCClF_2$ + Cl reaction (left). For the former reaction, the available experimental values are also reported.

Table 2. Comparison of the Arrhenius Parameters for the Reaction between $CH_2ClCClF_2$ and OH[a]

reference	T (K)	Arrhenius rate expression	E_a	experimental technique/theoretical method
ref 13[b]	250−350	$3 \times 10^{-12} \exp[-(1578)/T]$	3.14	FP-RF
this work	200−1000	$5.63 \times 10^{-12} \exp[-(1661/T)]$	3.30	CVT/μOMT
	200−1000	$5.75 \times 10^{-12} \exp[-(1689/T)]$	3.35	μVT/μOMT
ref 15	295−788	$(8.53 \pm 4.06) \times 10^{-19}\ T^{2.28} \exp[-(937 \pm 296)/T]$	1.86 ± 0.59	PLP-LIF
this work	200−1000	$4.10 \times 10^{-19}\ T^{2.28} \exp[-(706/T)]$	1.40	CVT/μOMT
	200−1000	$4.45 \times 10^{-19}\ T^{2.28} \exp[-(756/T)]$	1.50	μVT/μOMT

[a]Activation energy (E_a) in kcal mol^{-1}. [b]Reported uncertainties for preexponential factor, exponential factor, and activation energy: (+6, −1), (+400, −230), (0.79, −0.46).

Information (SI) collects the full list of values for all of the applied methods (TST, CVT, μVT, CVT/μOMT, and μVT/μOMT). For the reaction between HCFC-132b and the OH radical, the available experimental data are also reported. The results with SCT transmission coefficients are neither listed nor plotted for reaction R1 because they were computed always higher than the LCT ones, so they coincided within the whole temperature range here considered with the μOMT.

For reaction R1, the rate constants obtained at 298.15 K within the μVT and CVT framework and accounting for microcanonically optimized multidimensional tunneling (μOMT) are $k_{OH}^{\mu VT/\mu OMT} = 1.57 \times 10^{-14}$ cm^3 molecule^{-1} s^{-1} and $k_{OH}^{CVT/\mu OMT} = 1.72 \times 10^{-14}$, respectively. Both values are in excellent agreement with experimental measurements by Fang et al.[15] and Watson et al.,[13] who obtained a rate constant k_{OH} of 1.61×10^{-14} and 1.50×10^{-14} cm^3 molecule^{-1} s^{-1}, respectively. In contrast, the rate constant determined by Jeong et al.[14] ($k_{OH} = 2.95 \times 10^{-14}$ cm^3 molecule^{-1} s^{-1}), is about 50% larger than our theoretical results as well as than the experimental ones from refs 13 and 15. This may be due to the presence of impurities in the $CH_2ClCClF_2$ sample used in the experiments carried out in ref 14. For this reason, the rate coefficients determined by Jeong et al.[14] are not included in Figure 4.

As can be appreciated from Figure 4, $k_{OH}^{CVT/\mu OMT}$ and $k_{OH}^{\mu VT/\mu OMT}$ are both in excellent agreement with the experimental outcomes over the whole temperature range, with deviations within a factor of 0.75−1.06 and 0.74−0.97, respectively, compared to the most recent experimental results.[15] On the contrary, from the supporting Table S2, it can be observed that TST, CVT, and μVT underestimate the rate constants at all temperatures, especially in the temperature range 200−400 K because they neglect the contribution from tunneling effects, which are significant for the H-abstraction reaction. It should be noticed that, as expected, the variational effect (defined as the ratio between variational CVT and conventional TST rate constants) is not significant for this reaction, ranging from 0.75 at 200 K to 0.89 at 1000 K. Furthermore, it is worth mentioning that the CVT and μVT rate constants are similar at all temperatures.

For reaction R2, neither experimental nor theoretical data are available to compare. The rate constants calculated by TST, CVT, CVT/μOMT, μVT/μOMT, CVT/SCT, and μVT/SCT are collected in Table S2 in the Supporting Information (SI). From this table, it can be observed that the CVT and μVT values are similar at all temperatures, whereas TST rate constants are slightly higher than CVT and μVT rate constants at low temperatures, but the differences between them become smaller with increasing temperature, thus suggesting that the variational effect is only important at low temperatures. Tunneling effects are also significant only at lower temperatures (200−300 K), with the μOMT and SCT transmission coefficients at $T = 200$ K being 1.9 and 1.6, respectively. The μOMT transmission coefficient is found to be slightly higher than the SCT one at all of the temperatures, thus reflecting that the dominant tunneling mechanism in reaction R2 is the large-curvature tunneling.

3.2.4. Arrhenius Parameters. Arrhenius parameters obtained by different experimental techniques are listed in Table 2, where they are compared with the theoretical counterparts by the different theoretical methods employed in this work for reaction R1. The theoretical rate coefficients were also fitted using the two-parameter Arrhenius equations. Even though we do not recommend two-parameter Arrhenius fits in general, we present them in Table 2 simply as a way to make comparisons with the

https://doi.org/10.1021/acsearthspacechem.3c00025
ACS Earth Space Chem. 2023, 7, 892−900

results obtained by Watson et al.[13] For the $CH_2ClCClF_2$ + Cl reaction, the parameters of the modified Arrhenius expression, eq 5, are fitted to the calculated (CVT/μOMT, μVT/μOMT, CVT/SCT, μVT/SCT) rate constants in the temperature range of 200−1000 K, the corresponding values being summarized in Table 3.

Table 3. Modified Arrhenius Expressions for the $CH_2ClCClF_2$ + Cl Reaction Obtained in the 200−1000 K Temperature Range[a]

Arrhenius rate expression	E_a	theoretical method
$2.22 \times 10^{-18}\ T^{2.42} \exp[-(1070/T)]$	2.12	CVT/μOMT
$1.90 \times 10^{-18}\ T^{2.42} \exp[-(1038/T)]$	2.06	μVT/μOMT
$2.35 \times 10^{-18}\ T^{2.42} \exp[-(1116/T)]$	2.21	CVT/SCT
$2.01 \times 10^{-18}\ T^{2.42} \exp[-(1084/T)]$	2.15	μVT/SCT

[a]Activation energy (E_a) in kcal mol^{-1}.

3.3. Atmospheric Lifetime. It is generally assumed that the tropospheric lifetime of HCFCs can be estimated by considering that their removal from the atmosphere occurs mainly through reaction with OH and Cl radicals. In that sense, the overall rate of removal τ_{eff} can be expressed as

$$\frac{1}{\tau_{eff}} = \frac{1}{\tau_{Cl}} + \frac{1}{\tau_{OH}} \quad (7)$$

where $\tau_{Cl} = (k_{Cl} \times [Cl])^{-1}$ and $\tau_{OH} = (k_{OH} \times [OH])^{-1}$. Using the values of $k_{OH}^{\mu VT/\mu OMT} = 1.57 \times 10^{-14}$ cm^3 molecule^{-1} s^{-1} and $k_{Cl}^{\mu VT/\mu OMT} = 5.65 \times 10^{-14}$ cm^3 molecule^{-1} s^{-1} calculated at 298.15 K and the latest global average atmospheric [OH] and [Cl] concentrations of 1.09×10^6 and 1.0×10^4 molecule cm^{-3}, respectively,[69,70] the atmospheric lifetime for $CH_2ClCClF_2$ is estimated to be around 1.9 years. Obviously, when using the average global concentration of Cl, the contribution of reaction R2 for the removal of $CH_2ClCClF_2$ (HCFC-132b) from the atmosphere appears negligible because of the larger OH column density. However, in coastal areas, the scenario may be different since the Cl concentration is found to be much higher. Hence, the contribution from the reaction against Cl radicals is crucial for the determination of the atmospheric lifetime of $CH_2ClCClF_2$ (HCFC-132b), especially at the marine boundary layer.

4. CONCLUSIONS

HCFC-132b ($CH_2ClCClF_2$) has been newly detected in the atmosphere with a sub-ppt concentration and growing trend over the last decade, in opposition to the current international regulations that prohibit the use of ozone-depleting substances. With this premise, the present work aimed at investigating the reaction mechanism and kinetics of the H-abstraction reactions of $CH_2ClCClF_2$ initiated by the OH and Cl radicals, being this the entry step involved in the main atmospheric degradation pathway. The reactive potential energy surface and the related reaction and activation energies have been computed by using an accurate and cost-effective strategy relying on a hybrid CCSD(T)-based composite scheme/density functional theory computational protocol. In particular, a triple-slash dual-level approach to direct dynamics using the interpolated optimized corrections methodology at the jChS//B2PLYP-D3(BJ)/jun-cc-pV(T+d)Z///M06-2X-D3/jun-cc-pV(T+d)Z level has been adopted for simulating reaction kinetics. The rate constants have been calculated by using both CVT and μVT theories augmented through a microcanonically optimized multidimensional tunneling correction (μOMT) over the 200−1000 K temperature range. For the OH-initiated reaction, the kinetic rate constants have been found to be in perfect agreement with the available experimental data, with deviations being within a factor of 0.74−0.97.

The H-abstraction reaction initiated by the Cl atom has been investigated here for the first time. The overall reaction pathway mirrors that of the OH-initiated process, even though the latter has been computed to be exothermic by about −20 kcal mol^{-1}, while the exothermicity has been predicted around −5 kcal mol^{-1} when the reaction is initiated by Cl. From the computed rate constants, the following three-parameter Arrhenius expression (in cm^3 molecule^{-1} s^{-1}) in the temperature range of 200−1000 K has been derived: $k_{Cl} = 2.01 \times 10^{-18}\ T^{2.42} \exp[-(1084/T)]$. The obtained results show that at room temperature, the H-abstraction by Cl is about 3.6 times faster than the OH-initiated reaction. This suggests that, despite the lower atmospheric abundance of Cl, even this removal process can be of some relevance in determining the overall HCFC-132b atmospheric lifetime, especially in those environments characterized by increased levels of Cl (e.g., the marine boundary layer).

The present results not only provide reliable kinetic data with experimental accuracy but also present the application of an accurate yet cost-effective computational strategy to model gas-phase reactions involving this class of molecules that is being applied to HCFC-132b as well. The subsequent atmospheric processing of the radical produced by the initiation step, currently investigated in our group, will be the subject of an upcoming publication as well as a detailed characterization of HCFC-132b spectroscopic properties, particularly in the infrared region, being of relevance for understanding its contribution to global warming.

■ ASSOCIATED CONTENT

Supporting Information

The Supporting Information is available free of charge at https://pubs.acs.org/doi/10.1021/acsearthspacechem.3c00025.

Cartesian coordinates and harmonic vibrational frequencies of equilibrium geometries at the B2PLYP-D3(BJ)/jun-cc-pV(T+d)Z level of theory; thermal rate constants obtained with TST, CVT, μVT, and CVT, μVT including the SCT and μOMT approximations for tunneling for reactions R1 and R2 (PDF)

■ AUTHOR INFORMATION

Corresponding Author

Nicola Tasinato − *Scuola Normale Superiore, I-56126 Pisa, Italy*; orcid.org/0000-0003-1755-7238; Email: nicola.tasinato@sns.it

Authors

Nadjib Rais − *Scuola Normale Superiore, I-56126 Pisa, Italy; IUSS Scuola Universitaria Superiore, I-27100 Pavia, Italy*

Zoi Salta − *Scuola Normale Superiore, I-56126 Pisa, Italy*; orcid.org/0000-0002-7826-0182

Complete contact information is available at: https://pubs.acs.org/10.1021/acsearthspacechem.3c00025

Notes

The authors declare no competing financial interest.

■ ACKNOWLEDGMENTS

The SMART@SNS Laboratory (http://smart.sns.it) is acknowledged for providing high-performance computing facilities. This work has been supported by Scuola Normale Superiore (grant no. SNS22_A_FE_TASINATO). This paper and related research have been conducted during and with the support of the Italian inter-university Ph.D. course in sustainable development and climate change (link: www.phd-sdc.it).

■ REFERENCES

(1) Downie, D. L. *The Vienna Convention, Montreal Protocol and Global Policy to Protect Stratospheric Ozone*; Taylor & Francis: Oxford, 2012.
(2) Molina, M. J.; Rowland, F. S. Stratospheric sink for chlorofluoromethanes-chlorine atom catalyzed destruction of ozone. *Nature* **1974**, *249*, 810−815.
(3) Pinnock, S.; Hurly, M.; Shine, K. P.; Wallington, T. J.; Smyth, T. J. Radiative forcing of climate by hydrochlorofluorocarbons and hydrofluorocarbons. *J. Geophys. Res.* **1995**, *100*, 23227−23238.
(4) Vollmer, M. K.; Mühle, J.; Henne, S.; Young, D.; et al. Unexpected nascent atmospheric emissions of three ozone-depleting hydrochlorofluorocarbons. *Proc. Natl. Acad. Sci. U.S.A.* **2021**, *118*, No. e2010914118.
(5) *COWI Consult Consulting Engineers and Planners AS. Reduction of CFC Consumption—Anex Report*. Nordic Council of Ministers: Copenhagen, 1989.
(6) Hedenstrom, O. *Conditions for Reducing CFC Emission in Connection with Manufacture of Expanded Foam and Reduction of CFC-Release by Dry Cleaning, Degreasing and Drying*; Prikon AB for Statens Naturvardsvek, 1987.
(7) U.S. Department of State. *Chlorofluorocarbon Chemical Substitutes*; EPA: Washington, DC, 1986.
(8) Anders, M. W. Metabolism and toxicity of hydrochlorofluorocarbons: current knowledge and needs for the future. *Environ. Health Perspect.* **1991**, *96*, 185−191.
(9) Deviney, M. L., Jr.; Felsing, W. A. Some Compressibility Relations of 1,2-Dichloro-1,1-difluoroethane. *J. Am. Chem. Soc.* **1957**, *79*, 4915−4917.
(10) Cross, J. B.; Lielmezs, J. Thermodynamic Functions for 1,2-Dichloro-1,1-difluoroethane. *J. Chem. Eng. Data* **1967**, *12*, 75−76.
(11) Smith, P. H.; Kilroy, W. P.; James, S. D. Conductance off Electrolytes in 1,2-Dlchloro-1,1-diffluoroethane. *J. Chem. Eng. Data* **1984**, *29*, 284−285.
(12) Rodrigues, G. P.; Ventura, E.; Do Monte, S. A.; Barbatti, M. UV-photoexcitation and ultrafast dynamics of HCFC−132b (CF_2ClCH_2Cl). *J. Comput. Chem.* **2016**, *37*, 675−683.
(13) Watson, R. T.; Ravishankara, A. R.; Machado, G.; Wagner, S.; Davis, D. D. A Kinetics Study of the Temperature Dependence of the Reactions of OH($^2\Pi$) with CF_3CHCl_2, CF_3HClF, and CF_2ClCH_2Cl. *Int. J. Chem. Kinet.* **1979**, *11*, 187−197.
(14) Jeong, K.-M.; Hsu, K.-J.; Jeffries, J. B.; Kaufman, F. Kinetics of the reactions of hydroxyl with ethane, 1,1,1-trichloroethane, 1,1,2-trichloroethane, 1,1-difluoro-1,2-dichloroethane, and 1,1,1,2-tetrafluoroethane. *J. Phys. Chem. A* **1984**, *88*, 1222−1226.
(15) Fang, T. D.; Taylor, P. H.; Berry, R. J. Kinetics of the Reaction of OH Radicals with CH_2ClCF_2Cl and CH_2ClCF_3 over an Extended Temperature Range. *J. Phys. Chem. A* **1999**, *103*, 2700−2704.
(16) Sander, S. P.; Abbatt, J.; Barker, J. R.; Burkholder, J. B.; Friedl, R. R.; Golden, D. M.; Huie, R. E.; Kolb, C. E.; Kurylo, M. J.; Moortgat, G. K.; Orkin, V. L.; Wine, P. H. *Chemical Kinetics and Photochemical Data for Use in Atmospheric Studies Evaluation Number 16*; Jet Propulsion Laboratory: Pasadena, 2011.
(17) Ammann, M.; Cox, R. A.; Crowley, J. N.; Jenkin, M. E.; Mellouki, A.; Rossi, M. J.; Troe, J.; Wallington, T. J. *IUPAC Task Group on Atmospheric Chemical Kinetic Data Evaluation*; IUPAC, 2014.
(18) Calvert, J. G.; Derwent, R. G.; Orlando, J. J.; Tyndall, G. S.; Wallington, T. J. *Mechanisms of Atmospheric Oxidation of the Alkanes*; Oxford University Press: New York, 2008.
(19) Truhlar, D. G. The Reaction Path in Chemistry: Current Approaches and Perspectives. In *Direct Dynamics Method for the Calculation of Reaction Rates*; Heidrich, D., Ed.; Springer: Dordrecht, 1995; pp 229−255.
(20) Hu, W.-P.; Truhlar, D. G. Factors Affecting Competitive Ion−Molecule Reactions: ClO- + C_2H_5Cl and C_2D_5Cl via E2 and SN2 Channels. *J. Am. Chem. Soc.* **1996**, *118*, 860−869.
(21) Truhlar, D. G.; Garrett, B. C.; Klippenstein, S. J. Current Status of Transition-State Theory. *J. Phys. Chem. B* **1996**, *100*, 12771−12800.
(22) Truhlar, D. G.; Garrett, B. C. Variational transition-state theory. *Acc. Chem. Res.* **1980**, *13*, 440−448.
(23) Truhlar, D. G. Tunneling in Molecules: Nuclear Quantum Effects from Bio to Physical Chemistry. In *Semiclassical Multidimensional Tunneling Calculations*; Kaestner, J.; Kozuch, S., Eds.; RSC Publishing: Cambridge, 2021; pp 261−282.
(24) Zhao, Y.; Truhlar, D. G. The M06 suite of density functionals for main group thermochemistry, thermochemical kinetics, non-covalent interactions, excited states, and transition elements: two new functionals and systematic testing of four M06 functionals and 12 other functionals. *Theor. Chem. Acc.* **2008**, *120*, 215−241.
(25) Grimme, S.; Antony, J.; Ehrlich, S.; Krieg, H. A consistent and accurate ab initio parametrization of density functional dispersion correction (DFT-D) for the 94 elements H-Pu. *J. Chem. Phys.* **2010**, *132*, No. 154104.
(26) Papajak, E.; Zheng, J.; Xu, X.; Leverentz, H. R.; Truhlar, D. G. Perspectives on Basis Sets Beautiful: Seasonal Plantings of Diffuse Basis Functions. *J. Chem. Theory Comput.* **2011**, *7*, 3027−3034.
(27) Barone, V.; Ceselin, G.; Fusè, M.; Tasinato, N. Accuracy Meets Interpretability for Computational Spectroscopy by Means of Hybrid and Double-Hybrid Functionals. *Front. Chem.* **2020**, *8*, No. 584203.
(28) Salta, Z.; Segovia, M. E.; Katz, A.; Tasinato, N.; Barone, V.; Ventura, O. N. Isomerization and Fragmentation Reactions on the [C2SH4] Potential Energy Surface: The Metastable Thione S-Methylide Isomer. *J. Org. Chem.* **2021**, *86*, 2941−2956.
(29) Page, M.; McIver, J. W., Jr. On evaluating the reaction path Hamiltonian. *J. Chem. Phys.* **1988**, *88*, 922−935.
(30) Chuang, Y.-Y.; Truhlar, D. G. Reaction-Path Dynamics in Redundant Internal Coordinates. *J. Phys. Chem. A* **1998**, *102*, 242−247.
(31) Spada, L.; Tasinato, N.; Bosi, G.; Vazart, F.; Barone, V.; Puzzarini, C. On the competition between weak OH···F and CH···F hydrogen bonds, in cooperation with CH···O contacts, in the difluoromethane − tert-butyl alcohol cluster. *J. Mol. Spectrosc.* **2017**, *337*, 90−95.
(32) Salta, Z.; Tasinato, N.; Lupi, J.; Boussessi, R.; Balbi, A.; Puzzarini, C.; Barone, V. Exploring the Maze of C2N2H5 Radicals and Their Fragments in the Interstellar Medium with the Help of Quantum-Chemical Computations. *ACS Earth Space Chem.* **2020**, *4*, 774−782.
(33) Ceselin, G.; Salta, Z.; Bloino, J.; Tasinato, N.; Barone, V. Accurate Quantum Chemical Spectroscopic Characterization of Glycolic Acid: A Route Toward its Astrophysical Detection. *J. Phys. Chem. A* **2022**, *126*, 2373−2387.
(34) Grimme, S. Semiempirical hybrid density functional with perturbative second-order correlation. *J. Chem. Phys.* **2006**, *124*, No. 034108.
(35) Grimme, S.; Ehrlich, S.; Goerigk, L. Effect of the damping function in dispersion corrected density functional theory. *J. Comput. Chem.* **2011**, *32*, 1456−1465.
(36) Smith, D. G. A.; Burns, L. A.; Patkowski, K.; Sherrill, C. D. Revised Damping Parameters for the D3 Dispersion Correction to Density Functional Theory. *J. Phys. Chem. Lett.* **2016**, *7*, 2197−2203.
(37) Tasinato, N. What are the Spectroscopic Properties of HFC-32? Answers from DFT. *Int. J. Quantum Chem.* **2014**, *114*, 1472−1485.
(38) Puzzarini, C.; Bloino, J.; Tasinato, N.; Barone, V. Accuracy and Interpretability: The Devil and the Holy Grail. New Routes across Old Boundaries in Computational Spectroscopy. *Chem. Rev.* **2019**, *119*, 8131−8191.

https://doi.org/10.1021/acsearthspacechem.3c00025
ACS Earth Space Chem. 2023, 7, 892−900

(39) Boussessi, R.; Ceselin, G.; Tasinato, N.; Barone, V. DFT meets the segmented polarization consistent basis sets: Performances in the computation of molecular structures, rotational and vibrational spectroscopic properties. *J. Mol. Struct.* **2020**, *1208*, No. 127886.
(40) Tasinato, N.; Pietropolli Charmet, A.; Ceselin, G.; Salta, Z.; Stoppa, P. In Vitro and In Silico Vibrational−Rotational Spectroscopic Characterization of the Next-Generation Refrigerant HFO-1123. *J. Phys. Chem. A* **2022**, *126*, 5328−5342.
(41) Barone, V.; Lupi, J.; Salta, Z.; Tasinato, N. Development and Validation of a Parameter-Free Model Chemistry for the Computation of Reliable Reaction Rates. *J. Chem. Theory Comput.* **2021**, *17*, 4913−4928.
(42) Alessandrini, S.; Barone, V.; Puzzarini, C. Extension of the "Cheap" Composite Approach to Noncovalent Interactions: The jun-ChS Scheme. *J. Chem. Theory Comput.* **2020**, *16*, 988−1006.
(43) Helgaker, T.; Klopper, W.; Koch, H.; Noga, J. Basis-set Convergence of Correlated Calculations on Water. *J. Chem. Phys.* **1997**, *106*, 9639−9646.
(44) Møller, C.; Plesset, M. S. Note on an Approximation Treatment for many-electron Systems. *Phys. Rev.* **1934**, *46*, 618−622.
(45) Hu, W.-P.; Liu, Y.-P.; Truhlar, D. G. Variational Transition State Theory and Semiclassical Tunneling Calculations with Interpolated Corrections: A New Approach to Interfacing Electronic Structure Theory and Dynamics for Organic Reactions. *J. Chem. Soc., Faraday Trans.* **1994**, *90*, 1715−1725.
(46) Garrett, B. C.; Truhlar, D. G. Generalized transition state theory. Classical mechanical theory and applications to collinear reactions of hydrogen molecules. *J. Phys. Chem. C* **1979**, *83*, 1052−1079.
(47) Garrett, B. C.; Truhlar, D. G. Criterion of minimum state density in the transition state theory of bimolecular reactions. *J. Chem. Phys.* **1979**, *70*, 1593−1598.
(48) Liu, Y.-P.; Lu, D.-H.; González-Lafont, A.; Truhlar, D. G.; Garrett, B. C. Direct dynamics calculation of the kinetic isotope effect for an organic hydrogen-transfer reaction, including corner-cutting tunneling in 21 dimensions. *J. Am. Chem. Soc.* **1993**, *115*, 7806−7817.
(49) Skodje, R. T.; Truhlar, D. G.; Garrett, B. C. A general small-curvature approximation for transition-state-theory transmission coefficients. *J. Phys. Chem. D* **1981**, *85*, 3019−3023.
(50) Skodje, R. T.; Truhlar, D. G.; Garrett, B. C. Vibrationally adiabatic models for reactive tunnelling. *J. Chem. Phys.* **1982**, *77*, 5955−5976.
(51) Lu, D.-h.; Truong, T. N.; Melissas, V. S.; Lynch, G. C.; Liu, Y.-P.; Garrett, B. C.; Steckler, R.; Isaacson, A. D.; Rai, S. N.; Hancock, G. C.; Lauderdale, J. G.; Joseph, T.; Truhlar, D. G. POLYRATE 4: A new version of a computer program for the calculation of chemical reaction rates for polyatomics. *Comput. Phys. Commun.* **1992**, *71*, 235−262.
(52) Liu, Y.-P.; Lynch, G. C.; Truong, T. N.; Lu, D.-H.; Truhlar, D. G.; Garrett, B. C. Molecular modeling of the kinetic isotope effect for the [1,5]-sigmatropic rearrangement of cis-1,3-pentadiene. *J. Am. Chem. Soc.* **1993**, *115*, 2408−2415.
(53) Truhlar, D. G.; Isaacson, A. D.; Garrett, B. C. Generalized Transition State Theory. In *Theory of Chemical Reaction Dynamics*; Baer, M., Ed.; CRC Press: Boca Raton, 1985; Vol. 4, pp 65−137.
(54) Fernández-Ramos, A.; Ellingson, A.; Meana-Pañeda, R.; Marques, J. M. C.; Truhlar, D. G. Symmetry numbers and chemical reaction rates. *Theor. Chem. Acc.* **2007**, *118*, 813−826.
(55) Garrett, B. C.; Truhlar, D. G.; Wagner, A. F.; Dunning, T. H., Jr. Variational transition state theory and tunneling for a heavy−light−heavy reaction using an ab initio potential energy surface. ^{37}Cl+H(D) ^{35}Cl→H(D) ^{37}Cl+^{35}Cl. *J. Chem. Phys.* **1983**, *78*, 4400−4413.
(56) Garrett, B. C.; Abusalbi, N.; Kouri, D. J.; Truhlar, D. G. Test of variational transition state theory and the least-action approximation for multidimensional tunneling probabilities against accurate quantal rate constants for a collinear reaction involving tunneling into an excited state. *J. Chem. Phys.* **1985**, *83*, 2252−2258.
(57) Garrett, B. C.; Joseph, T.; Truong, T. N.; Truhlar, D. G. Application of the large-curvature tunneling approximation to polyatomic molecules: Abstraction of H or D by methyl radical. *Chem. Phys.* **1989**, *136*, 271−293.
(58) Fernández-Ramos, A.; Truhlar, D. G. Improved algorithm for corner-cutting tunneling calculations. *J. Chem. Phys.* **2001**, *114*, 1491−1496.
(59) Fernández-Ramos, A.; Truhlar, D. G. A New Algorithm for Efficient Direct Dynamics Calculations of Large-Curvature Tunneling and Its Application to Radical Reactions with 9−15 Atoms. *J. Chem. Theory Comput.* **2005**, *1*, 1063−1078.
(60) Fernández-Ramos, A.; Miller, J. A.; Klippenstein, S. J.; Truhlar, D. G. Modeling the Kinetics of Bimolecular Reactions. *Chem. Rev.* **2006**, *106*, 4518−4584.
(61) Frisch, M. J.; Trucks, G. W.; Schlegel, H. B.; Scuseria, G. E.; Robb, M. A.; Cheeseman, J. R.; Scalmani, G.; Barone, V.; Petersson, G. A.; Nakatsuji, H.et al. *Gaussian 16*, revision C.01; Gaussian Inc.: Wallingford, CT, 2016.
(62) Zheng, J.; Bao, J. L.; Meana-Pañeda, R.; Zhang, S.; Lynch, B. J.; Corchado, J. C.; Chuang, Y.-Y.; Fast, P. L.; Hu, W.-P.; Liu, Y.-P.; Lynch, G. C.; Nguyen, K. A.; Jackels, C. F.; Fernandez Ramos, A.; Ellingson, B. A.; Melissas, V. S.; Villà, J.; Rossi, I.; Coitiño, E. L.; Pu, J.; Albu, T. V.; Ratkiewicz, A.; Steckler, R.; Garrett, B. C.; Isaacson, A. D.; Truhlar, D. G. *Polyrate-version 2017-C*; University of Minnesota: Minneapolis, MN, 2017.
(63) Zheng, J.; Bao, J. L.; Zhang, S.; Corchado, J. C.; Meana-Pañeda, R.; Chuang, Y.-Y.; Coitiño, E. L.; Ellingson, B. A.; Truhlar, D. G. *Gaussrate 17*; University of Minnesota: Minneapolis, MN, 2017.
(64) Ruscic, B.; Bross, D. H. *Active Thermochemical Tables (ATcT)*; Argonne National Laboratory, 2021. ATcT.anl.gov.
(65) Pollak, E.; Pechukas, P. Symmetry numbers, not statistical factors, should be used in absolute rate theory and in Broensted relations. *J. Am. Chem. Soc.* **1978**, *100*, 2984−2991.
(66) Sekušak, S.; Liedl, K. R.; Rode, B. M.; Sabljić, A. Reaction-Path Dynamics of Hydroxyl Radical Reactions with Ethane and Haloethanes. *J. Phys. Chem. A* **1997**, *101*, 4245−4253.
(67) Sekušak, S.; Sabljić, A. The role of complexes in hydrogen abstraction from haloethanes by the hydroxyl radical. A case of guided reactions. *Chem. Phys. Lett.* **1997**, *272*, 353−360.
(68) Masgrau, L.; González-Lafont, A.; Lluch, J. M. Effect of a complex formation on the calculated low-pressure rate constant of a bimolecular gas-phase reaction governed by tunneling. *J. Comput. Chem.* **1999**, *20*, 1685−1692.
(69) Li, M.; Karu, E.; Brenninkmeijer, C.; Fischer, H.; Lelieveld, J.; Williams, J. Tropospheric OH and stratospheric OH and Cl concentrations determined from CH_4, CH_3Cl, and SF_6 measurements. *NPJ Clim. Atmos. Sci.* **2018**, *1*, No. 29.
(70) Wingenter, O. W.; Kubo, M. K.; Blake, N. J.; Smith, T. W.; Blake, D. R.; Rowland, F. S. Hydrocarbon and halocarbon measurements as photochemical and dynamical indicators of atmospheric hydroxyl, atomic chlorine, and vertical mixing obtained during Lagrangian flights. *J. Geophys. Res.: Atmos.* **1996**, *101*, 4331−4340.

https://doi.org/10.1021/acsearthspacechem.3c00025
ACS Earth Space Chem. 2023, 7, 892−900